Journal of Magnetism and Magnetic Materials xxx (xxxx) xxxx

Contents lists available at ScienceDirect

Journal of Magnetism and Magnetic Materials

journal homepage: www.elsevier.com/locate/jmmm

Research articles

# Promising spintronics: Mn-based Heusler alloys $Mn_3Ga$, $Mn_2YGa$ (Y = V, Nb, Ta), ScMnVGa

Li Fan, Feng Chen, Chun-mei Li, Xun Hou, Xin Zhu, Jiang-lei Luo, Zhi-Qian Chen*

*School of Materials and Energy, Southwest University, Chongqing 400715, PR China*

ARTICLE INFO

*Keywords:*
Density functional theory (DFT)
Heusler alloys
Gapless half-metallicity
Spin gapless semiconductors
Magnetism and tetragonal distortion

ABSTRACT

High spin-polarized materials are expected for the development of spintronic devices. In this work, we are aiming to find new spintronic materials in Mn-based binary, ternary and quaternary Heusler alloys by using the first-principles calculations. We investigated structures, electronic properties, magnetic, tetragonal distortion and mechanic properties of $Mn_3Ga$, $Mn_2YGa$ (Y = V, Nb, Ta) and ScMnVGa. The results show that $Mn_3Ga$, ScMnVGa type-I, and type-II have lower energy in antiferromagnetic (AFM) states than ferromagnetic (FM) and paramagnetic (NM). $Mn_2YGa$ (Y = V, Nb, Ta) compounds are more stable in FM states. The results of electronic and magnetic properties indicate that $Mn_3Ga$ is a gapless half-metallic antiferromagnet (Gapless HM-AFM). $Mn_2VGa$ and $Mn_2NbGa$ belong to gapless half-metallic ferrimagnets (Gapless HM-FE). $Mn_2TaGa$ is ferrimagnets. ScMnVGa type-I is half-metallic antiferromagnets (HM-AFM) and type-II belongs to spin gapless semiconductors with AFM (SGSs-AFM). Inspired by Ferromagnetic shape memory alloys (FAMAs), we performed tetragonal deformation of those compounds, and we predicted that $Mn_3Ga$, $Mn_2YGa$ (Y = V, Nb, Ta) have possible martensitic transformations. Finally, the mechanical stability and elastic properties of above-mentioned in both cubic and tetragonal structures were discussed in detail.

## 1. Introduction

Spintronics is considered to be one of the most promising subjects in the information age because spintronic devices use not only the state of charge but electronic spin to transfer and store information, which speeds up information transmission and reduces energy losses. The findings of Giant Magnetoresistance (GMR), Colossal Magnetoresistance (CMR) and Tunnel Magnetoresistance (MGR) accelerate the development of spintronics. Despite great potential advantages, spintronics still faces some challenges, such as, generate high spin injectors. However, the discovery of half-metallic ferrimagnet has improved this problem, which is an ideal semiconductor spin-injection source due to it has 100% spin polarizability. Among different half-metallic materials, Heusler alloys are prominent especially owing to high Curie temperature and flexible electronic structures [1,2]. Since De Groot et al. [3] discovered the half-metallic ferromagnets of NiMnSb, while they were calculating the energy band using the plane-wave method, this intermetallic materials with unusual electronic structures arouse people's attention.

In the big family of Heusler alloys, Co-based Heusler alloys [4–6] usually show magnetism, and the source of this property is direct interaction between Co-Co atoms. Cu-based Heusler alloys [7–9] are typical representative of non-magnetic elements show ferromagnetic after high-ordered, Pd-based Heusler alloys [10,11] which contain rare-earth elements is superconducting, $Ni_2Mn$-based Heusler alloys [12–17] have both ferromagnetic properties and thermoelastic martensitic transformation, which realizing magnetic-field-induced strain, shape memory effect, magnetoresistance effect and other application functions. At present, most research focuses on ternary Mn-based Heusler alloys, and they usually behave ferromagnetic or ferromagnetic [18–21]. Actually, besides half-metallic ferromagnets and ferrimagnets, half-metallic antiferromagnets also worthy of study. Not only it has 100% spin polarizability, but its total magnetic moment is zero. Thus, it means that when HM-AFMs are applied to spintronic devices, and those alloys will get the feature of the low-stray field and low energy loss. HM-AFMs were discovered in Heusler alloys [22] and perovskite compounds [23]. Besides, the martensitic transformation was found in some Mn-based Heusler alloys [24–26].

In addition to traditional half-metallic materials, some new materials which have fully spin-polarized have entered people's field of vision: spin gapless semiconductors (SGSs) and gapless half-metals (Gapless HM). Wang et al. [27] originally discovered SGSs in 2008. They are sub-class of gapless semiconductor, in which VBM (valence band maximum) and CBM (the conduction band minimum) touch each

* Corresponding author.
*E-mail address:* chen_zq@swu.edu.cn (Z.-Q. Chen).

https://doi.org/10.1016/j.jmmm.2019.166060
Received 22 March 2019; Received in revised form 24 October 2019; Accepted 25 October 2019
Available online 05 November 2019
0304-8853/ 

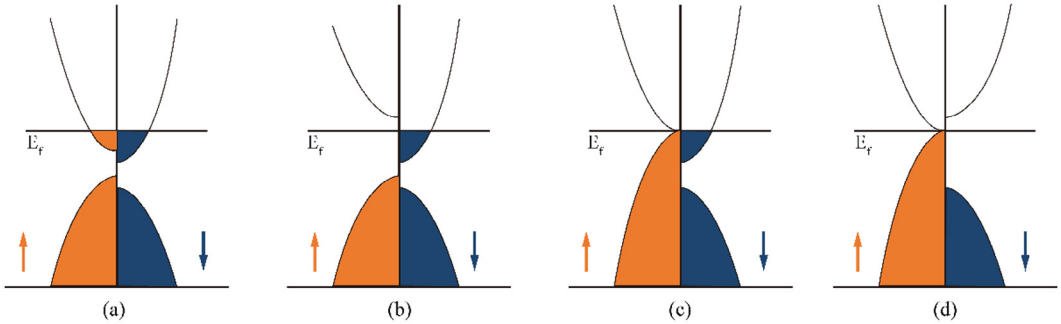


**Fig. 1.** Schematic plots of band structures for various spintronic materials (a) ferromagnetic metal, (b) half-metals, (c) gapless half-metal, (d) spin gapless semiconductors.

other at Femi level (Fig. 1(d)). For SGSs, at least one of CBM and the VBM is fully spin-polarized. The combine of semiconductor and spin-polarized endue a lot of interesting properties. For examples, no energy required to excite electrons from VB to CB, and excited carriers are fully spin-polarized. Thus it produces SGSs unique transformation properties: coexistence of high Curie temperature and high resistance. Besides, carriers mobility of SGSs is about 2–4 orders of magnitude than traditional semiconductors, due to their quadratic or linear energy band dispersion [28]. What's more, SGSs is sensitive to outside effects such as magnetic field and pressure, so they can turn for many application in spintronics, optics, and sensors [29]. At present SGSs have been verified by experiment, according to synthesis $Mn_2CoAl$ [30]. Inspired by SGSs, Du et al. [31] proposed another new half-metallic material, Gapless half-metallic (Gapless HM) or zero-gap HMMs, by experimentally synthesizing $Fe_2CoSi$. One of Gapless HM's spin channels is gapless (Fig. 1(c)), while another channel behaves metallic properties, thus Gapless HMMs result in 100% spin polarizability. $Fe_2CoFe$ has measured Curie temperature is very high (1038 K). Furthermore, with the temperature increasing, there is a positive to negative magnetoresistance, and this can attribute to dominant carriers which are changed from the gapless channel to metallic channel at Femi level. Fig. 1. shows schematic plots of band structures for various spintronic materials: ferromagnetic metal (FM), half-metal (HM), gapless half-metal (Gapless HM), spin gapless semiconductor (SGS).

In general, as mention above HM-FM, HM-AFM, SGSs, and Gapless HM have 100% spin polarizability at Femi level; thus, they all important spintronic materials. To further application of spintronics, studying on these materials seem to especially necessary. Before this, there have been some related researches, Gao et al. [32] discover Gapless HM when they studied binary Heusler alloys. Gapless HM and SGSs are also found in a small number of ternary or quaternary Heusler alloys [30,33,34]. In this paper, the first-principles calculation of Mn-based binary, ternary and quaternary Heusler alloys is carried out, and we investigated electronic structure, magnetic properties, martensitic transformation and elastic properties in detail.

## 2. Calculation details

We have employed first-principles calculations based on density functional theory (DFT) [35,36], Mn-based Heusler alloys $Mn_3Ga$, $Mn_2YGa$ (Y = V, Nb, Ta) and ScMnVGa was investigated. All calculations are performed by CASTEP (Cambridge Serial Total Energy package) code [37]. Generalized gradient approximation (GGA) [38] with Perdew–Burke–Ernzerhof (PBE) [39] formula was carry out to represent the exchange-correlation between electrons, and Ultrasoft and On the fly pseudopotentials are selected to describe electronic – iron interaction for cubic and tetragonal structure, respectively. Mn $3d^54s^2$, V $3s^23p^63d^34s^2$, Nb $4s^24p^64d^45s^1$, Ta $5d^36s^2$, Ga $3d^{10}\ 4s^24p^1$, Sc $3\,s^2\ 3p^63d14s^2$ Pseudoatomic configuration are treated as valence electrons. The convergence test is performed with cut-off energy from 350 to 550 eV within a step 25 eV, and k-points is setting from $5 \times 5 \times 5$ to$15 \times 15 \times 15$, we finally choose 500 eV cut-off energy and $12 \times 12 \times 12$ k-points in the Brillouin zone for accurate results. Convergence energy tolerance of self-consistence is checked within $1 \times 10^{-6}$ eV/atom, and force on each atom of the unit cell is less than 0.02 eV/Å.

## 3. Results and discussion

### 3.1. Structural properties

There are many kinds of Heusler alloys, so there are several ways to categorize them. For example, according to the central element types, they are include Fe-based, Co-based, Ni-based, Pd-based etc. Heusler alloys. For the number of elements, they contain binary, ternary, and quaternary Heusler alloy. In this work, we investigate Mn-based binary, ternary and quaternary Heusler alloys. The space group for binary and quaternary Heusler alloy is *F4_3m* (No. 216 in the table of space group). For ternary, it is *Fm_3m* (No. 225), which is composite by four face-centered cubic (fcc). Fig. 2 shows schematic plots for m. Table 1 lists the specific space group and Wyckoff position.

To find more stable ground states, we performed total energy (E) as a function of volume for paramagnetic, ferrimagnetic and ferromagnetic states, and fit into Birch-Murnaghan's equilibrium equation. (ScMnVGa type-III behaves paramagnetic, so we do not have further research.) Fig. 2. displays the results. From Fig. 2, we can find out that $Mn_3Ga$ is more stable in antiferromagnetic states than paramagnetic and ferrimagnetic, cause blue triangles which represent ferrimagnetic are under blank squares and red rounds. $Mn_2YGa$ (Y = V, Nb, Ta) have lower energy in ferromagnetic states, while ScMnVGa type-I, type-II are more stable in antiferromagnetic states. Hence, in the following chapters, we only discuss these stable states. Table 2 lists the lattice constants after optimized and bulk modulus obtained by fitting the curves. The results of Gao et al. [32] showed that the lattice constant of $Mn_3Ga$ is 5.82 Å. The experiment result [21] of $Mn_2VGa$ show that its lattice constant is 5.907 Å, while calculation results of Christoph Klewe et al. [40] are 5.805 Å. Our calculation result is 5.848 Å that is close to the experimental values. Most of the compounds in this study have not yet been synthesized, so it is necessary to discuss their formation energy and cohesive energy to judge the stability of these compounds. The cohesive energy and formation energy are calculated based on the following Eqs. (1) and (2).

$$\Delta E_{coh} = \left(E_{Mn_2YGa} - aE_{Mn}^{atom} - bE_{Y}^{atom} - cE_{Ga}^{atom}\right)/(a+b+c) \quad (1)$$

$$\Delta E_{form} = \left(E_{Mn_2YGa} - aE_{Mn}^{solid} - bE_{Y}^{solid} - cE_{Ga}^{solid}\right)/(\mathrm{a}+\mathrm{b}+\mathrm{a}) \quad (2)$$

where $\Delta E_{coh}$ $\boldsymbol{\Delta E_{coh}}$ and $\boldsymbol{\Delta E_{form}}$ refer to cohesive and formation energies respectively; $E_{Mn_2YGa}$ $\Delta E_{coh} E_{CsYO_2} E_{CsYO_2}$ is the total energy of the compound at equilibrium lattice constant; $E^{atom}$ represent $E^{atom}$ the energy of the single Sc, Mn, Y and Ga atom and $E^{solid}E^{solid}$ is the total energy of

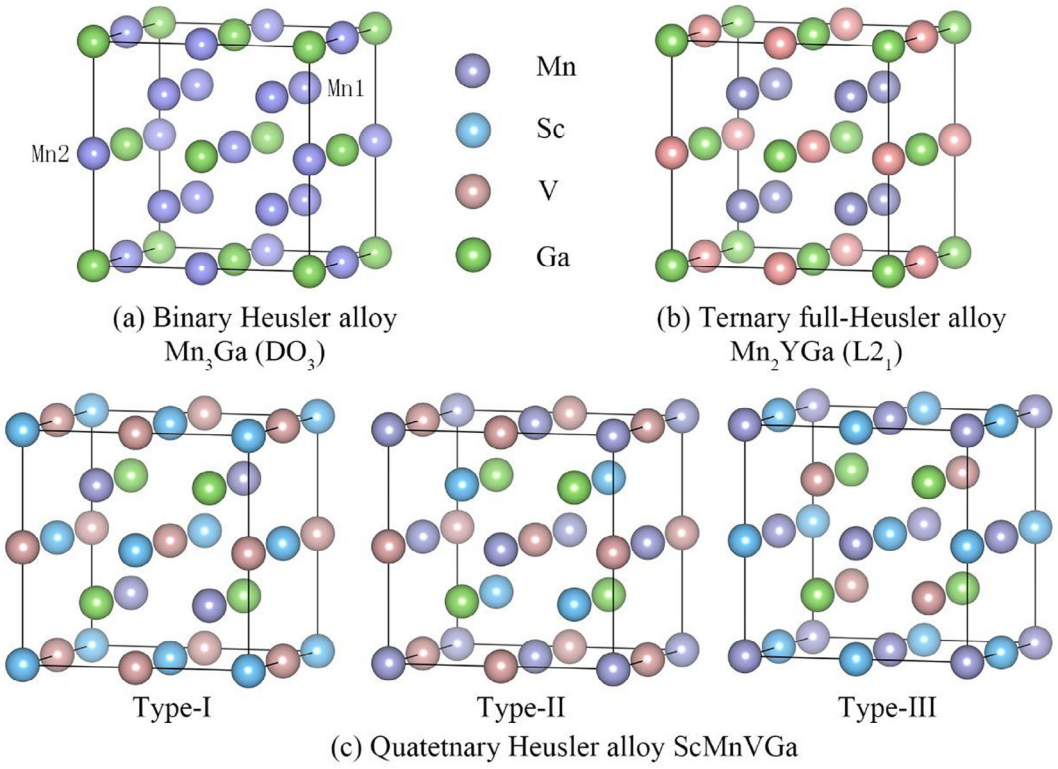


**Fig. 2.** The crystal structure of (a) binary Heusler alloy $Mn_3Ga$ ($DO_3$-type), (b) ternary full-Heusler alloy $Mn_2YGa$ ($Hg_2CuTi$-type) and (c) quaternary Heusler alloy ScMnVGa (Y-type).

the per atom for Sc, Mn, Y and Ga. The results are listed at Table 2, in which we can see that the values of both cohesive energy and formation energy for those six compounds are negative, and this means that they all have thermodynamic stability.

### 3.2. Electronic structure and magnetic properties

To investigate electronic structures, we calculated band structures and density of states of $Mn_3Ga$, $Mn_2YGa$ (Y = V, Nb, Ta) and ScMnVGa (type-I and type-II) at equilibrium lattice constants. To make the results clear, all calculations in this chapter are performed by unit cells, which are display at Figs. 3 and 4. Fig. 3 has shown band structures in both spin up and spin down, which are distinguished by the red arrow symbols, spin up is listed to the left and spin down is to the right side. We can see from $Mn_2TaGa$, both spin up and spin down have across Femi level, but they are not asymmetry. Therefore, $Mn_2TaGa$ exhibits magnetism but it is not a half-metal; it belongs to a magnetic metallic material. The spin-up of ScMnVGa type-I across Femi level which exhibits metallicity, while a band gap is observed at spin down which shows semiconductor properties. This phenomenon leads to ScMnVGa Type-I manifests half-metallicity, and its spin polarization reaches 100%. The interesting phenomenon appears to band structures of $Mn_3Ga$ and $Mn_2VGa$, one of their spin channels shows metallicity, on another channel, VBM and CBM touch each other at high-symmetry point and the Fermi level falls within a zero-width gap. They leave a gapless band structure. Thus these two compounds are gapless (zero-

**Table 2**
Calculation of the lattice constants (a), bulk parameters (B) and cohesive energies ($E_c$) and formation energies ($E_f$) of $Mn_3Ga$, $Mn_2YGa$ (Y = V, Nb, Ta) and ScMnVGa (type-I and type-II).

| Compounds | a (Å) | B (GPa) | $E_c$ (eV) | $E_f$ (eV) |
|---|---|---|---|---|
| $Mn_3Ga$ | 5.872<br>5.82[a] | | −0.387 | −0.179 |
| $Mn_2VGa$ | 5.845<br>5.907[b]<br>5.808[c] | 135 | −0.716 | −0.394 |
| $Mn_2NbGa$ | 6.013 | 168 | −0.577 | −0.362 |
| $Mn_2TaGa$ | 6.210 | 205 | −0.576 | −0.343 |
| ScMnVGa Type-I | 6.342 | 123 | −0.875 | −0.341 |
| ScMnVGa Type-II | 6.372 | 89 | −0.815 | −0.282 |
| ScMnVGa Type-III | 6.360 | | −0.875 | −0.314 |

[a] Gao et al. (Ref. [32]) calculation.
[b] Ramesh Kumar et al. (Ref. [21]) experiment.
[c] Christoph Klewe et al. (Ref. [40]) calculation.

**Table 1**
The atomic arrangements in full-Heusler alloys, $DO_3$-type binary Heusler alloys and quaternary Heusler alloys.

| Variants | Structure | Wyckoff positions | | | |
|---|---|---|---|---|---|
| | | A (0, 0, 0) | B (1/4, 1/4, 1/4) | C (1/2, 1/2, 1/2) | D (3/4, 3/4, 3/4) |
| Binary Heusler alloys $Mn_3Ga$ | $DO_3$ | Mn | Mn | Mn | Ga |
| Full-Heusler alloys $Mn_2YGa$ | $L2_1$ | Mn | Mn | Y | Ga |
| Quaternary Heusler alloys ScMnVGa | Type-I | Sc | Mn | V | Ga |
| | Type-II | Mn | Sc | V | Ga |
| | Type-III | Mn | V | Sc | Ga |

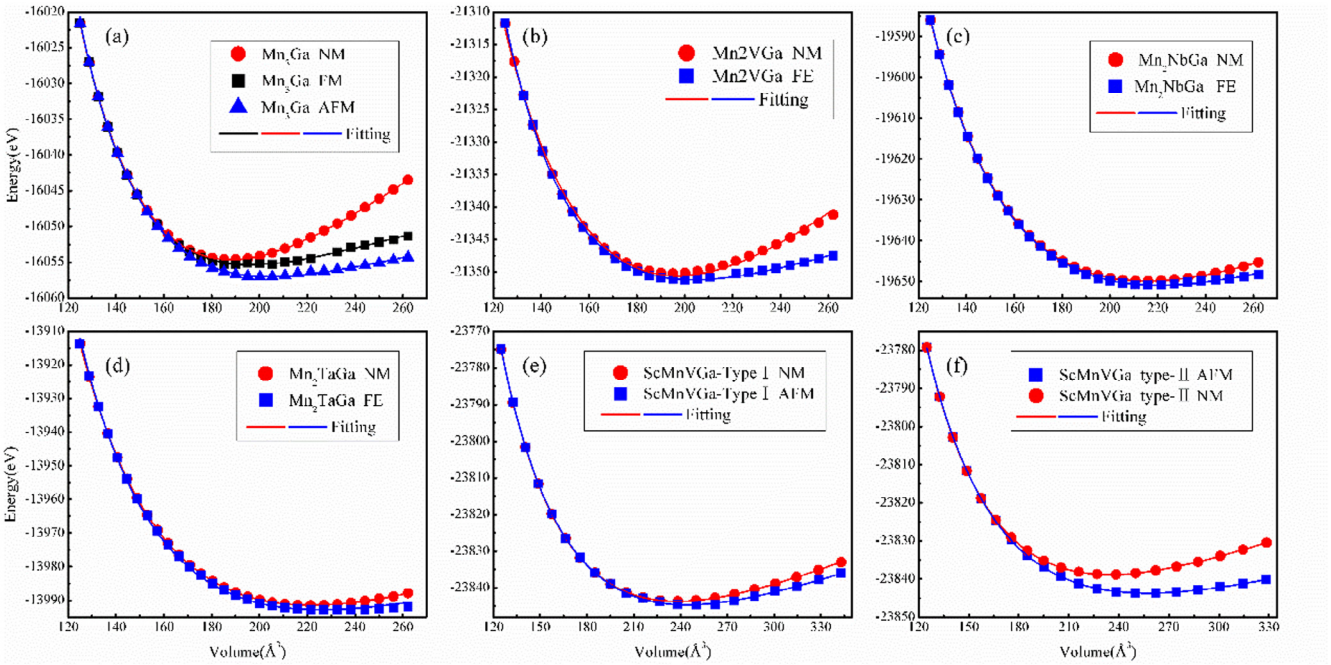


**Fig. 3.** Total energy as a function of volume for the (a) $Mn_3Ga$, (b) $Mn_2VGa$, (c) $Mn_2NbGa$, (d) $Mn_2TaGa$, (e) ScMnVGa type-I and (f) ScMnVGa type-II in NM, FM, FE, AFM states.

gap) half-metal materials at equilibrium lattice constants. Similarly, there is a small gap between $Mn_2NbGa$'s CBM and VBM in spin up channel, and resulted in a direct gap. Different from the gapless half-metal materials predicted in other references [31,41], VBM and CBM of these three compounds are in contact with each other at the same high symmetry point. This highly dispersive energy band or even near-linear-dispersive appears in quaternary Heusler alloys composed of rare earth elements [42]. Another structure that deserves our attention is ScMnVGa type-II, which has a indirect band gap on the spin down channel. While in the spin-up energy band, at the high symmetry point Gamma point, there is a band gap between the conduction band and the valence band, and the highest point of the valence band is in touch without crossing the Fermi level. Therefore, ScMnVGa Type-II can be classified as spin gapless semiconductor (SGS). Spin gapless semiconductors are also present in other Heusler alloys [30,34]. Comparing the difference between the three compounds of $Mn_2YGa$ (Y = V, Nb, Ta), it considers that the Ta element contains 4f orbital, which makes the electron cloud arrangement between atoms more compact.

We can see from the Fig. 4 that the energy between −10 eV and 6 eV of the six compounds, the 4p orbital of Ga atom mainly contributes the spin-up and spin-down density states. For $Mn_3Ga$, the density of states of spin up around Femi level is mostly arises from Mn1 and Mn2 atoms. DOS of $Mn_2YGa$ (Y = V, Nb, Ta) around Femi level major comes from hybridization between and Mn and Y atom. The DOS of ScMnYGa (type-I and type-II) near Femi level is mainly contributed by V atom. From 0 eV to 6 eV, the DOS is origin form Mn atom, V atom, and Sc atom, and the peaks of the partial density of the three atoms correspond to each other, indicating that there is a strong hybrid among them. Since Mn atom mainly contribute to the density of states of $Mn_3Ga$ at the Fermi level, the source of magnetic and half-metallicity of the $Mn_3Ga$ compound are the 3d orbitals of Mn atoms. In the $Mn_2YGa$ (Y = V, Nb, Ta) on the right side of Fig. 4., the density of states at the Fermi level is mainly the 3d orbital contribution of the Y atom and the Mn atom; thus, magnetic and half-metallic properties mostly come from Mn atoms and Y atoms. Among the Type-I and Type-II of ScMnVGa, the main source of magnetic, half-metallic and spin gapless semiconductivity is mainly contributed by hybridization of the 3d orbit of Mn atom, V atom and Sc atom.

Positive values of DOS are chosen as majority spin electrons and negative values are minority ones.

The total magnetic moments, atom magnetic moments, magnetic states and physical nature are listed in Table 3. As we can see from Table 3, the total magnetic moments of $Mn_2YGa$ (Y = V, Nb, Ta) are 1.99μB, 2.00μB, 4.26μB, respectively, and the magnetic moments of Y atoms are −0.82 μB, −0.30 μB and −0.90 μB, respectively, which are antiparallel to the magnetic moment of the Mn atom, so $Mn_2YGa$ (Y = V, Nb, Ta) exhibits ferrimagnetism. Combining the band structure results analysis, $Mn_2VGa$ and $Mn_2NbGa$ belong to the gapless half-metal ferrimagnetic material (Gapless HM-FE), while $Mn_2TaGa$ is ferromagnetic materials. The total magnetic moment of $Mn_3Ga$, ScMnVGa type-I, and ScMnVGa type-II is 0, and there are positive and negative values in the atomic magnetic moment, so these three compounds have antiferromagnetic properties. According to the results of band structures, $Mn_3Ga$ belongs to gapless half-metallic antiferromagnetic, ScMnVGa type-I belongs to half-metallic antiferromagnetic materials, and ScMnVGa type-II belongs to spin gapless semiconductor antiferromagnetic. To the best of our knowledge, most Heusler alloys satisfy the Slater-Pauling rule [43]: $M_{tot} = (Z - 24)$ or$M_{tot} = (Z - 18)$, where $M_{tot}$represents the total magnetic moment of the cell, Z is the total number of valence electrons, and 24 and 18 indicate that 12 and 9 orbitals are filled. The valence electron numbers of $Mn_3Ga$, $Mn_2VGa$, and $Mn_2NbGa$ are 22, 22, and 24, respectively, and the magnetic moments are 0 μB, 1.99 μB (close to 2.00), and 2.00 μB, respectively, so the three compounds satisfy the Slater-Pauling rules: $M_{tot} = (Z - 24)$. For ScMnVGa (type-I and type-II), they have 18 valence electrons, and total magnetic moments are zero, thus, they satisfy $M_{tot} = (Z - 18)$. This also proves on the other hand that these compounds are half-metallic.

### 3.3. Tetragonal deformation

The shape memory effect in Heusler alloys is a phase transition from austenite to martensite. The specific process is reflected in the anisotropic tetragonal structure becoming an isotropic cubic structure. At present, the main research method is Bain paths [44], which refers to the method of reversible order between the ordered $L2_1$ austenite and the $L1_0$ martensite phase during the tetragonal deformation process.

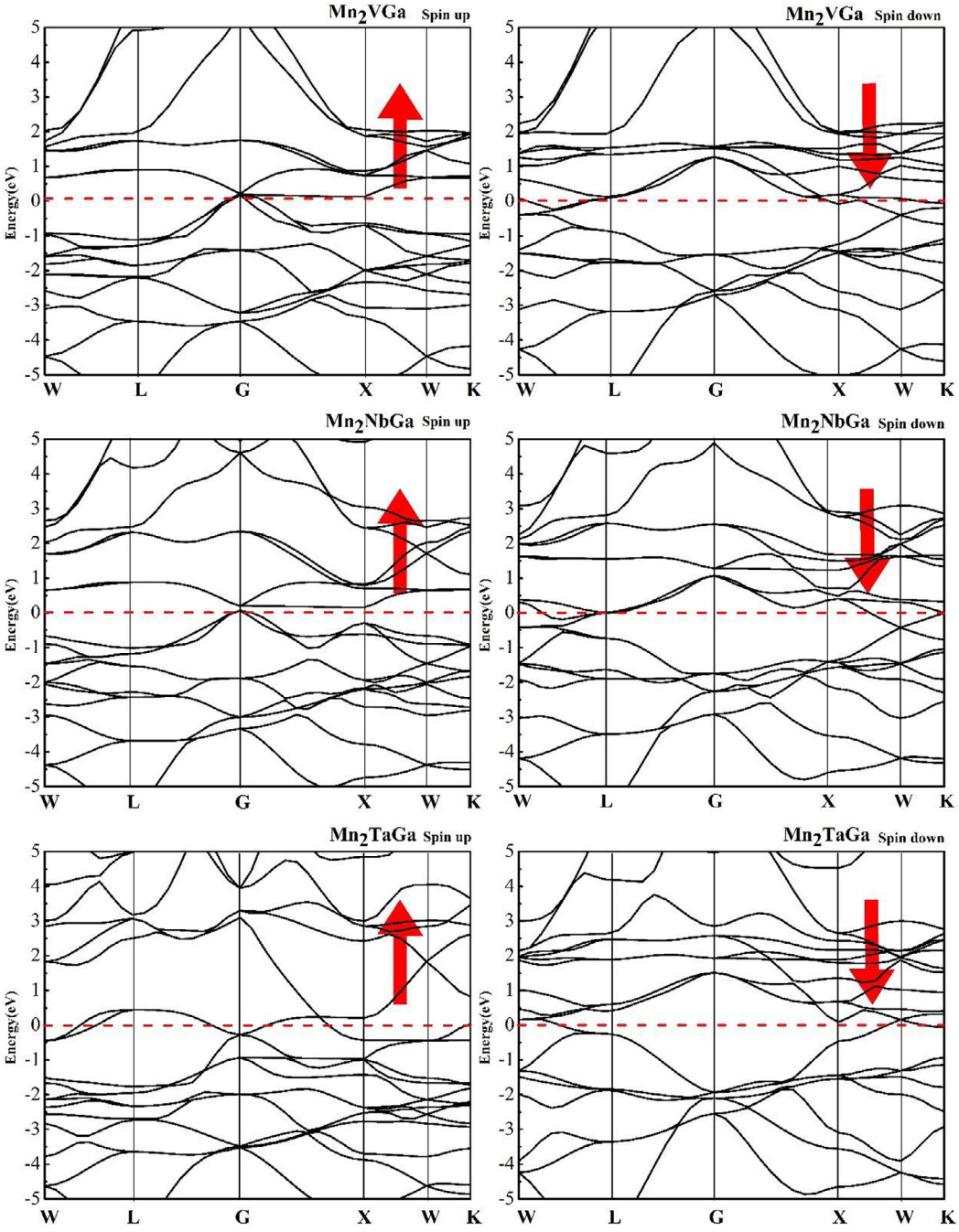


**Fig. 4.** The spin up and spin down band structures patterns of $Mn_3Ga$, $Mn_2VGa$, $Mn_2NbGa$ $Mn_2TaGa$, ScMnVGa Type-I and Type-II compounds at the equilibrium lattice parameters.

The Bain path method assumes that the cell volume does not change after the deformation is applied to the cubic phase, and then calculates the energy difference corresponding to c/a to estimate whether the compound is stable or metastable.

In this work, we calculated the energy of different c/a by tetragonal transformation of $Mn_3Ga$, $Mn_2YGa$ (Y = V, Nb, Ta) and ScMnVGa Type-I and type-II, the results are plotted in Fig. 5. To make the results clearer, we have drawn different ranges of Bain paths. The c/a variation range of Mn3Ga $Mn_2YGa$ (Y = V, Nb, Ta) and ScMnVGa Type-I and type-II are 0.90–1.48, 0.860–1.32, 0.88–1.32, 0.77–1.36, 0.8–1.48, 0.80–1.48, respectively. ΔE represents the difference between the energy at the different c/a and the energy at the $L2_1$ structure.

From Fig. 5 we can see that there is only one energy minimum value in ScMnVGa type- I and type-II, which is $L2_1$ structure. It means that the two compounds are the more stable in the cubic structures and there are no other phases. $Mn_3Ga$, $Mn_2VGa$, and $Mn_2TaGa$ have two lowest energy points, one locates at the $L2_1$ structure and another lies in $c/a > 1$. This indicated that stable phases are located at $c/a = 1.32$, $c/a = 1.44$ and $c/a = 1.44$, respectively. For $Mn_2NbGa$, there are two points with lower energy than $L2_1$, one locates at $c/a < 1$, and the other one located at $c/a > 1$. They illuminate that metastable phases exist in these energy local minima. In other words, we can predict that $Mn_3Ga$ and $Mn_2YGa$ (Y = V, Nb, Ta) compounds have a shape memory effect by applying external temperature and stress. Besides, we list the corresponding lattice constants of martensite phases in Table 4. Also, we can also see that $Mn_3Ga$ have the largest energy difference than

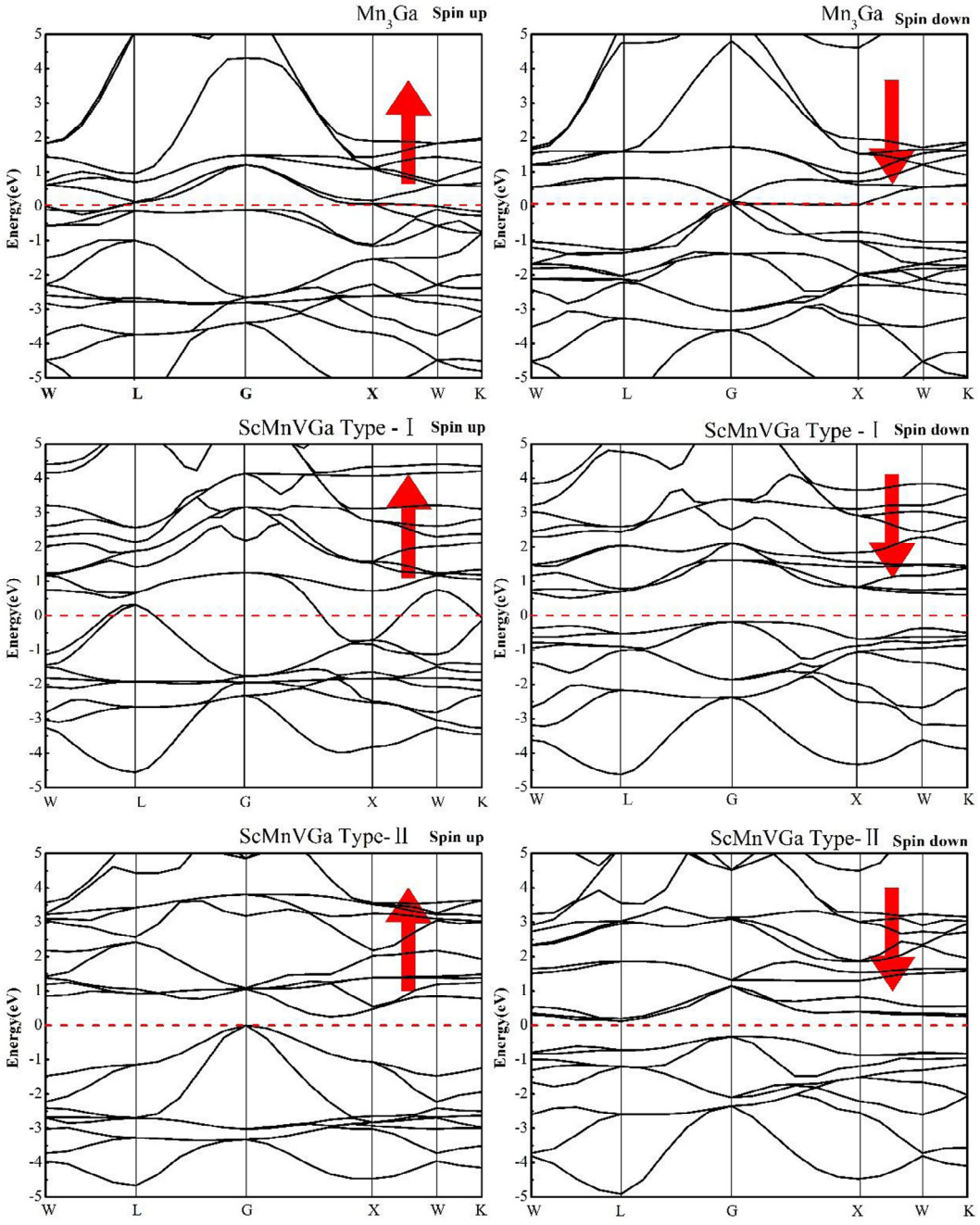


**Fig. 4.** (*continued*)

**Table 3**
Calculated total magnetic moments and the atomic magnetic moments ($M_{tot}$) per formula unit, magnetic states and physical nature for Heusler alloys, $Mn_3Ga$, $Mn_2YGa$ (Y = V, Nb, Ta), ScMnVGa Type-I and type-II.

| Compounds | $M_{tot}/\mu_B$ | $M_{Mn}/\mu_B$ | | $M_Y/\mu_B$ | $M_{Sc}/\mu_B$ | $M_{Ga}/\mu_B$ | Magnetic states | Physical nature |
|---|---|---|---|---|---|---|---|---|
| $Mn_3Ga$ | 0 | 1.45 ($Mn_1$) | −0.73 ($Mn_2$) | | | 0 | AFM | Gapless HM |
| $Mn_2VGa$ | 1.99 | 1.39 | | −0.82 | | 0.03 | FE | Gapless HM |
| | 2[a] | 1.50[a] | | −0.90[a] | | 0 | FE | |
| | 1.99[b] | 1.64[b] | | −1.20[b] | | | | |
| $Mn_2NbGa$ | 2.00 | 1.14 | | −0.30 | | 0.01 | FE | Gapless HM |
| $Mn_2TaGa$ | 4.26 | 2.57 | | −0.90 | | 0.01 | FE | Metallic |
| ScMnVGa Type-I | 0 | 2.35 | | −2.15 | −0.08 | −0.12 | AFM | HM |
| ScMnVGa Type-II | 0 | 1.56 | | −1.29 | −0.24 | −0.04 | AFM | SGSs |

[a] Ramesh Kumar et al. (Ref. [21]) experiment.
[b] Christoph Klewe et al. (Ref. [40]) calculation.

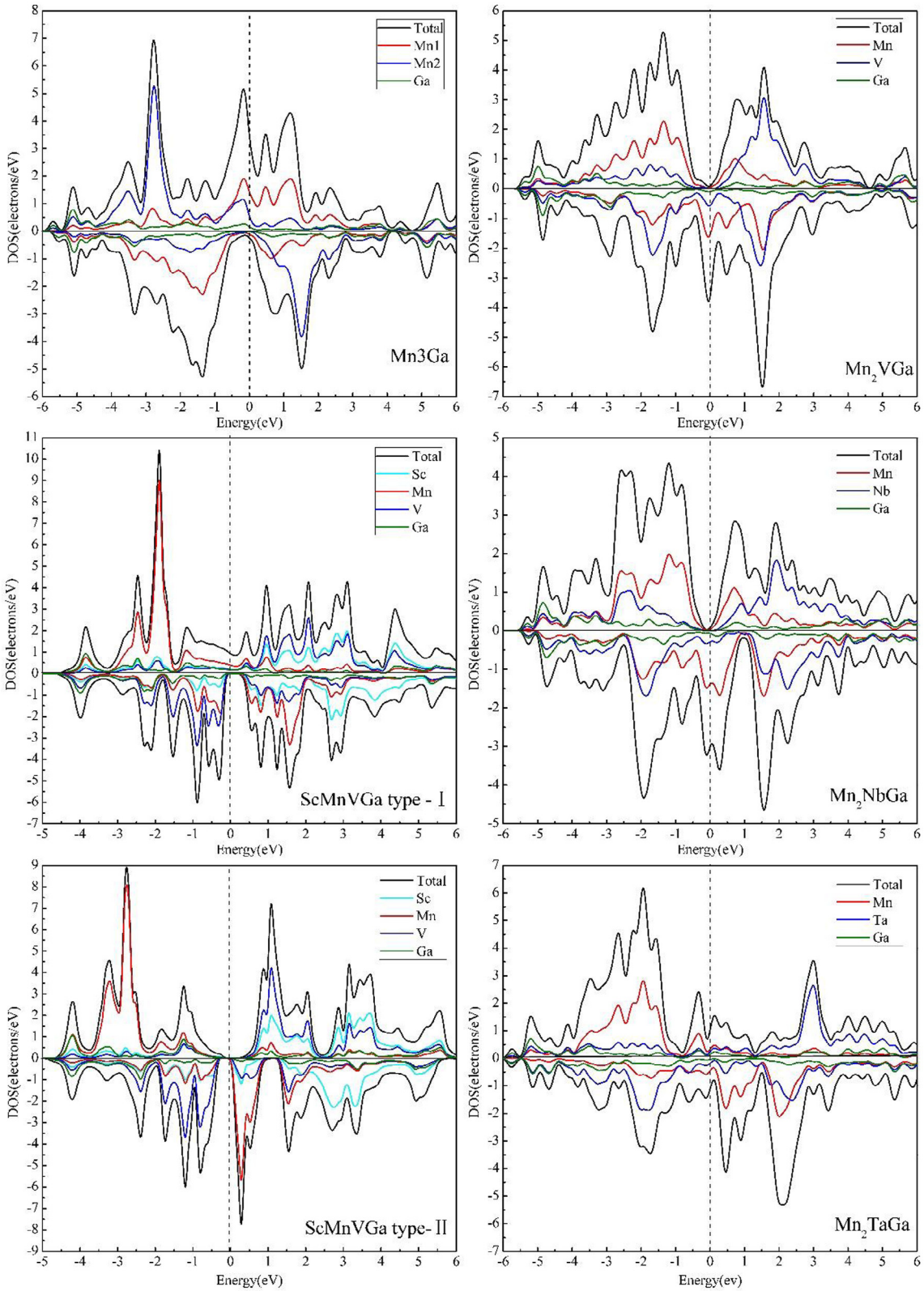


**Fig. 5.** The total density of states (TDOS) and the density of partial states (PDOS) of $Mn_3Ga$, $Mn_2YGa$ (Y = V, Nb, Ta) and ScMnVGa (type-I and type-II) at equipment lattice constants.

$Mn_2YGa$ (Y = V, Nb, Ta). Thus, we can predict that the martensite phase of $Mn_3Ga$ is relatively stable and has a higher phase transition temperature than other compounds. At present, the experimentally synthesized $Mn_3Ga$ in references [45–47] is the almost tetragonal phase, which also shows that the tetragonal phase is more stable than the cubic phase. Table 4 lists the comparison between the calculation results of the $Mn_3Ga$ tetragonal structure and the experimental results. It can be seen from Table 4 that the theoretical calculation results are close to the experimental results, but there is a nearly 3% difference, which is mainly due to cell volume does not change after deformation

**Table 4**
Calculated lattice parameter (a, c) and space group of $Mn_3Ga$ and $Mn_2YGa$ (Y = V, Nb, Ta) in tetragonal phase.

| Compounds | | c/a | Space group | a (Å) | c (Å) |
|---|---|---|---|---|---|
| $Mn_3Ga$ | This work | 1.32 | *I4/mmm* | 3.790 | 7.065 |
| | Experiment[a] | | *I4/mmm* | 3.906 | 7.100 |
| | Experiment[b] | | I4/mmm | 3.904 | 7.088 |
| | Calculation[c] | | *I4/mmm* | 3.88 | 7.03 |
| $Mn_2VGa$ | | 1.14 | *I4/mmm* | 3.957 | 6.379 |
| $Mn_2NbGa$ | | 0.96 | *I4/mmm* | 4.311 | 5.852 |
| | | 1.16 | *I4/mmm* | 4.047 | 6.639 |
| $Mn_2TaGa$ | | 1.44 | *I4/mmm* | 4.116 | 6.635 |

[a] Experiment Rode et al. [46].
[b] Experiment Balke et al. [45].
[c] Calculation Wollmann et al. [48].

(See Fig. 6).

### 3.4. Elastic properties

Elastic properties are critical to technological applications, so it is necessary to study the hardness, stability, anisotropy and stiffness of materials. In this chapter, we will explore the elastic properties of $Mn_3Ga$, $Mn_2VGa$, $Mn_2NbGa$, $Mn_2TaGa$, ScMnVGa Type-I, and ScMnVGa Type-II cubic structures and tetragonal structures by calculating the elastic constants ($c_{ij}$). Due to the high symmetry of the cubic structure, there are only three independent elastic constants ($c_{11}$, $c_{12}$, $c_{14}$) among the 21 elastic constants, and the tetragonal structures (*I4/mmm*) have six independent elastic constants ($c_{11}$, $c_{33}$, $c_{44}$, $c_{66}$, $c_{12}$, $c_{13}$). The criteria for the stability of the cubic structures and the tetragonal structures are as follows:

Cubic crystal:

$$(c_{11} - c_{12}) > 0,\ c_{11} > 0,\ c_{44} > 0,\ (c_{11} + 2c_{12}) > 0$$

Tetragonal crystal:

$$(c_{11} - c_{12}) > 0,\ (c_{11} + c_{13} - 2c_{13}) > 0$$

$$c_{11} > 0, c_{13} > 0,\ c_{44} > 0,\ c_{66} > 0$$

$$(2c_{11} + c_{33} + 2c_{12} + 4c_{13}) > 0$$

The calculated elastic constants of the cubic structure and the tetragonal structure are listed in Table 5. According to the above criteria, we can conclude that the cubic structure of $Mn_3Ga$ does not satisfy the stability criterion ($c_{11} - c_{12} > 0$) while the tetragonal structure shows stability. This explains why the experimentally synthesized $Mn_3Ga$ is a tetragonal structure. The $Mn_2VGa$ and $Mn_2NbGa$ cubic structures and the tetragonal structures are both stable. The $Mn_2TaGa$ cubic structure is stable, while the tetragonal structure is unstable. The ScMnVGa type-I cubic structure is unstable ($c_{44} < 0$); the ScMnVGa Type- II cubic structure is stable. The elastic constants are usually for single crystals, and the alloy is usually polycrystalline, so we need to evaluate the corresponding elastic modulus of the polycrystal by Voigt- Reuss [49,50] approximation.

$$B = (c_{11} + 2c_{12})/3$$

$$G = (c_{11} - c_{12} + 3c_{44})/5$$

Other elastic moduli such as Young's modulus E and Poisson's ratio $\nu$ [51], universal anisotropy $A^U$index [52], can be obtained by the following formula:

$$E = (9GB)/(3B + G)$$

$$\nu = (3B - 2G)/(6B + 2G)$$

$$A^U = (5G_V/G_R) + (B_V/B_R) - 6$$

$G_V$, $G_R$ and $B_V$, $B_R$ are the bulk modulus and shear modulus of the Voigt and Reuss approximation, respectively.

Table 4 lists the elastic modulus of cubic and tetragonal structures of $Mn_3Ga$, $Mn_2YGa$ (Y = V, Nb, Ta), ScMnVGa Type-I, and ScMnVGa Type-II, from which we can analyze the mechanical properties of these compounds. The B/G is the parameter which is defined as the indicator of brittleness or ductility of a material. The value of the ratio is higher than1.75 indicates ductility, while lower than 1.75 refers to brittleness. The cubic and tetragonal structure, the B/G value is founded to be > 1.75 for the compounds of $Mn_3Ga$ (tetragonal), $Mn_2VGa$ (cubic), $Mn_2NbGa$ (cubic and tetragonal for c/a = 1.16), $Mn_2TaGa$ (cubic),

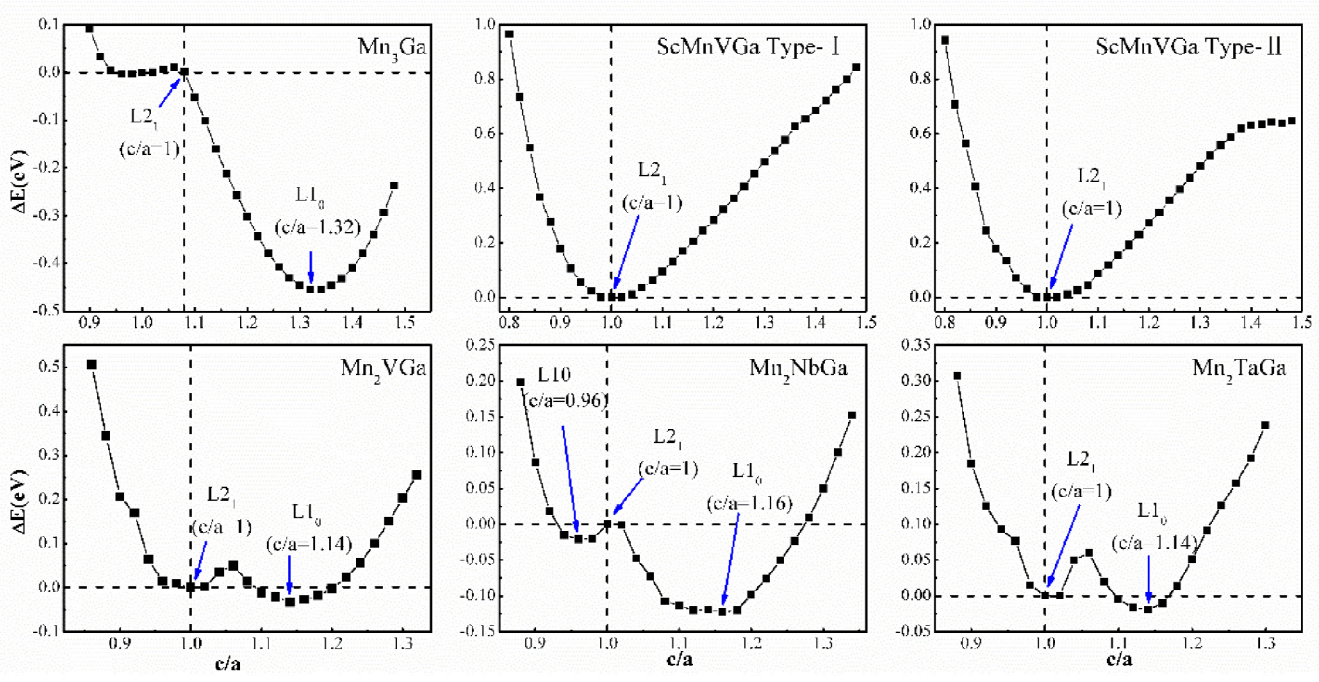


**Fig. 6.** The c/a dependences of energy difference for $Mn_3Ga$, $Mn_2YGa$ (Y = V, Nb, Ta) and ScMnVGa (type-I and type-II).

**Table 5**
Elastic constants ($c_{11}$, $c_{33}$, $c_{44}$, $c_{66}$, $c_{13}$, $c_{12}$) and elastic models: the bulk modulus B (GPa), shear modulus G (GPa), Young's modulus E (GPa), Poisson's ratio υ and universal anisotropy factor $A^U$ of cubic and tetragonal Heusler alloys of $Mn_3Ga$, $Mn_2YGa$ (Y = V, Nb, Ta) and ScMnVGa (type-Iand type-II).

Cubic

| Compounds | $c_{11}$ | $c_{12}$ | $c_{44}$ | $B$ | $G$ | $E$ | $\nu$ | $B/G$ | $A^U$ |
|---|---|---|---|---|---|---|---|---|---|
| $Mn_3Ga$ | 143.077 | 148.048 | 117.744 | 146.391 | | | | | |
| $Mn_2VGa$ | 242.245 | 146.498 | 123.674 | 178.413 | 84.536 | 219.14 | 0.297 | 2.110 | 1.16 |
| $Mn_2NbGa$ | 269.715 | 157.956 | 121.496 | 195.209 | 88.958 | 153.036 | 0.302 | 2.194 | 0.76 |
| $Mn_2TaGa$ | 205.427 | 117.915 | 124.160 | 147.085 | 81.780 | 206.98 | 0.265 | 1.799 | 1.42 |
| ScMnVGa Type-I | 114.668 | 45.564 | −87.136 | 68.598 | 68.598 | | | | |
| ScMnVGa Type-II | 120.656 | 76.496 | 93.310 | 91.216 | 52.779 | 61.294 | 0.257 | 1.728 | 2.95 |

Tetragonal

| Compounds | c/a | $c_{11}$ | $c_{33}$ | $c_{44}$ | $c_{66}$ | $c_{12}$ | $c_{13}$ | $B(GP_a)$ | $G(GP_a)$ | $B/G$ | $E(GPa)$ | $\nu$ | $A^U$ |
|---|---|---|---|---|---|---|---|---|---|---|---|---|---|
| $Mn_3Ga$ | 1.36 | 197.53 | 196.07 | 115.14 | 117.48 | 135.70 | 118.94 | 148.553 | 72.398 | 2.052 | 209.721 | 0.265 | 1.92 |
| $Mn_2VGa$ | 1.14 | 268.89 | 147.44 | 131.35 | 102.68 | 84.58 | 120.45 | 143.575 | 82.140 | 1.748 | 206.953 | 0.598 | 2.29 |
| $Mn_2NbGa$ | 0.96 | 219.65 | 224.02 | 109.70 | 13.28 | −28.05 | 82.38 | 99.359 | 61.183 | 1.624 | 152.291 | 0.2445 | 5.12 |
| | 1.16 | 265.17 | 207.25 | 126.592 | 114.040 | 103.542 | 128.705 | 161.723 | 91.351 | 1.770 | 230.628 | 0.264 | 0.86 |
| $Mn_2TaGa$ | 1.14 | 22.094 | 93.362 | 93.779 | 29.855 | −113.05 | 93.362 | 60.146 | 65.258 | | | | |

while they are less than 1.75 for the compounds of $Mn_2VGa$ (tetragonal), ScMnVGa type-II and $Mn_2NbGa$ (tetragonal for c/a-0.96). According to reference studies, when the value of Poisson's ratio is small (close to 0.1), corresponding to the covalent material, and when the value of Poisson's ratio is large (close to 0.25), it corresponds to the ionic material. From Table 5 we can see that the Poisson's ratios of both the tetragonal structure and the cubic structure are close to 0.25, so, they are all ionic materials [53]. The general elastic anisotropy $A^U = 0$ indicates that the single crystal exhibits isotropy, and the greater the deviation of $A^U$ from 0, the greater the degree of anisotropy of the crystal. It can be seen from the results in Table 5 that these compounds are all anisotropic materials with a large degree of anisotropy. In addition, the degree of anisotropy of the tetragonal structure is greater than that of the cubic structure.

## 4. Conclusion

In this paper, we calculated the structural properties, electronic structures, tetragonal deformation and mechanical properties of $Mn_3Ga$, $Mn_2YGa$ (Y = V, Nb, Ta), ScMnVGa type-I ScMnVGa type-II using first-principles calculations based on density functional theory. Our calculations show that $Mn_3Ga$, ScMnVGa type-I, and type-II are more stable in the antiferromagnetic state, and $Mn_2YGa$ (Y = V, Nb, Ta) is more stable in the ferrimagnetic state. ScMnVGa type-III is not magnetic. $Mn_3Ga$, $Mn_2YGa$ (Y = V, Nb, Ta) and ScMnVGa (type-I and type-II) have thermodynamic stability by calculation of cohesive and formation energy. The band structures results show that $Mn_2TaGa$ belongs to a ferrimagnetic magnet; ScMnVGa type-I exhibits half-metal antiferromagnetic. Besides, highly dispersed gapless half-metallicity occurs in $Mn_3Ga$, $Mn_2VGa$, and $Mn_2NbGa$ when they are at equilibrium lattice. More importantly, the band structure of ScMnVGa type-II shows that it belongs to spin gapless semiconductors (SGSs). The results of the TDOS and the PDOS show that the magnetic and half-metallic properties of the compounds are origins from the hybridization between the transition elements. Except for $Mn_2TaGa$, the regional compounds have a 100% spin polarizability and the magnetic moments are integers, satisfying the Slater-Pauling rule: $M_{tot} = (Z - 24)$ or $M_{tot} = (Z - 18)$. $Mn_3Ga$ and $Mn_2YGa$ (Y = V, Nb, Ta) have a shape memory effect because of the energy difference in the austenite phase to a martensite phase transition. The cubic structure of $Mn_3Ga$ does not satisfy the mechanical stability, but the tetragonal structure shows stability and the tetragonal structure exhibits ductility. The tetragonal structure and cubic structure of $Mn_2VGa$ are both stable and ductile, and the cubic and tetragonal structures of $Mn_2NbGa$ are mechanically stable. The cubic structure and the tetragonal structure of c/a = 1.16 exhibit ductility, and another tetragonal structure of c/a = 0.96 exhibits brittleness. The $Mn_2TaGa$ cubic structure is stable but the tetragonal structure is unstable, and the cubic structure is ductile. The ScMnVGa type-I cubic phase is unstable, and ScMnVGa type- II has mechanical stability and exhibits brittleness. $Mn_3Ga$, $Mn_2YGa$ (Y = V, Nb, Ta) and ScMnVGa (type-I and type-II) all exhibit anisotropy.

## Declaration of Competing Interest

The authors declare that they have no known competing financial interests or personal relationships that could have appeared to influence the work reported in this paper.

## Acknowledgements

This work was financially supported by the National Natural Science Foundation of China (No. 51601153) and the Fundamental Research Funds for the Central Universities (No. XDJK2018C004 and No. SWU115068).

## References

[1] C. Felser, G.H. Fecher, B. Balke, Spintronics: a challenge for materials science and solid-state chemistry, Angew. Chem. Int. Ed. 46 (2007) 668–699.
[2] K. Inomata, N. Ikeda, N. Tezuka, R. Goto, S. Sugimoto, M. Wojcik, E. Jedryka, Highly spin-polarized materials and devices for spintronics, Sci. Technol. Adv. Mater. 9 (2008) 014101.
[3] R.A.D. Groot, F.M. Mueller, P.G.V. Engen, K.H.J. Buschow, New class of materials: half-metallic ferromagnets, Phys. Rev. Lett. 50 (1983) 2024–2027.
[4] M. Kogachi, T. Fujiwara, S. Kikuchi, Atomic disorder and magnetic property in co-based Heusler alloys Co2MnZ (Z = Si, Ge, Sn), J. Alloys Compd. 475 (2009) 723–729.
[5] A. Aguayo, G. Murrieta, Density functional study of the half-metallic ferromagnetism in Co-based Heusler alloys Co2MSn (M = Ti, Zr, Hf) using LSDA and GGA, J. Magn. Magn. Mater. 323 (2011) 3013–3017.
[6] W. Leiper, C.G. White, J. Judah, C. Blaauw, Hyperfine fields of Fe impurities in the co-based heusler alloys Co2(Ti, Hf, V)Al, J. Magn. Magn. Mater. 15–8 (1980) 639–640.
[7] Y.V. Kudryavtsev, V.A. Oksenenko, N.N. Lee, Y.P. Lee, J.Y. Rhee, J. Dubowik, Effect of structural disorder on some physical properties of the Cu2MnAl Heusler alloy films, J. Appl. Phys. 97 (2005) 113903.
[8] U. Geiersbach, A. Bergmann, K. Westerholt, Structural, magnetic and magneto-transport properties of thin films of the Heusler alloys Cu2MnAl, Co2MnSi, Co2MnGe and Co2MnSn, J. Magn. Magn. Mater. 240 (2002) 546–549.
[9] Y.F. Wen, X.S. Zeng, Y.X. Ye, L.G. Yan, D.L. Wu, Q.D. Gou, L.L. Liu, First-principles calculations of acoustic and anharmonic properties of ferromagnetic Cu2MnZ (Z = Al and In) heusler alloys, J. Supercond. Nov. Magn. 31 (2018) 1847–1856.

[10] S.K. Malik, A.M. Umarji, G.K. Shenoy, Magnetic and Mössbauer studies on rare-earth-containing Heusler alloys Pd2RSn (R = Tb-Yb), Phys. B 31 (1985) 6971.
[11] R.L. Donaberger, C.V. Stager, Magnetic-structures of the rare-earth heusler alloys Pd2DySn and Pd2HoSn, J. Less-Common Met. 127 (1987) 93–98.
[12] V.A. Chernenko, E. Cesari, V.V. Kokorin, I.N. Vitenko, The development of new ferromagnetic shape-memory alloys in Ni-Mn-Ga system, Scrip. Metal. Mater. 33 (1995) 1239–1244.
[13] J.W. Dong, J.Q. Xie, J. Lu, C. Adelmann, C.J. Palmstrom, J. Cui, Q. Pan, T.W. Shield, R.D. James, S. McKernan, Shape memory and ferromagnetic shape memory effects in single-crystal Ni2MnGa thin films, J. Appl. Phys. 95 (2004) 2593–2600.
[14] A. Sozinov, A.A. Likhachev, N. Lanska, K. Ullakko, Giant magnetic-field-induced strain in NiMnGa seven-layered martensitic phase, Appl. Phys. Lett. 80 (2002) 1746–1748.
[15] P.J. Webster, K.R.A. Ziebeck, S.L. Town, M.S. Peak, Magnetic order and phase-transformation in Ni2MnGa, Philos. Mag. B 49 (1984) 295–310.
[16] K. Ullakko, J.K. Huang, C. Kantner, R.C. OHandley, V.V. Kokorin, Large magnetic-field-induced strains in Ni2MnGa single crystals, Appl. Phys. Lett. 69 (1996) 1966–1968.
[17] G.H. Wu, C.H. Yu, L.Q. Meng, J.L. Chen, F.M. Yang, S.R. Qi, W.S. Zhan, Z. Wang, Y.F. Zheng, L.C. Zhao, Giant magnetic-field-induced strains in Heusler alloy NiMnGa with modified composition, Appl. Phys. Lett. 75 (1999) 2990–2992.
[18] X.F. Dai, G.D. Liu, L.J. Chen, J.L. Chen, G.H. Wu, Mn2CoSb compound: structural, electronic, transport and magnetic properties, Solid State Commun. 140 (2006) 533–537.
[19] R. Weht, W.E. Pickett, Half-metallic ferrimagnetism in Mn2VAl, Phys. Rev. B 60 (1999) 13006–13010.
[20] Z. Ren, Y. Liu, S.T. Li, X.H. Zhang, H.Y. Liu, Site preference and electronic structure of Mn2RhZ (Z = Al, Ga, In, Si, Ge, Sn, Sb): a theoretical study, Mater. Sci-Poland. 34 (2016) 251–259.
[21] K.R. Kumar, N.H. Kumar, P.D. Babu, S. Venkatesh, S. Ramakrishnan, Investigation of atomic anti-site disorder and ferrimagnetic order in the half-metallic Heusler alloy Mn2VGa, J. Phys.: Condens. Matter 24 (2012) 336007.
[22] I. Galanakis, E. Sasioglu, High T-C half-metallic fully-compensated ferrimagnetic Heusler compounds, Appl. Phys. Lett. 99 (2011) 39-R.
[23] V. Pardo, W.E. Pickett, Compensated magnetism by design in double perovskite oxides, Phys. Rev. B 80 (2009) 1956–1960.
[24] H.Z. Luo, G.D. Liu, F.B. Meng, S.J. Li, W. Zhu, G.H. Wu, X.X. Zhu, C.B. Jiang, Electronic structure and magnetism of the Heusler alloy Mn2NiAl: a theoretical study of the shape-memory behavior, Phys. B 405 (2010) 3092–3095.
[25] Y.N. Duan, X.X. Fan, A. Kuduk, X.J. Du, Z.W. Zhang, Y.L. Song, Possible martensitic transformation and ferrimagnetic properties in Heusler alloy Mn2NiSn, J. Magn. Magn. Mater. 386 (2015) 102–106.
[26] Q.L. Fang, J.M. Zhang, X.M. Zhao, K.W. Xu, V. Ji, Magnetic properties and possible martensitic transformation in Mn2NiSi and Ni2MnSi Heusler alloys, J. Magn. Magn. Mater. 362 (2014) 42–46.
[27] X.L. Wang, Proposal for a new class of materials: spin gapless semiconductors, Phys. Rev. Lett. 100 (2008) 156404.
[28] X.X. Li, J.L. Yang, First-principles design of spintronics materials, Natl. Sci. Rev. 3 (2016) 365–381.
[29] X.L. Wang, S.X. Dou, C. Zhang, Zero-gap materials for future spintronics, electronics and optics, NPG Asia Mater. 2 (2010) 31–38.
[30] S. Ouardi, G.H. Fecher, C. Felser, J. Kubler, Realization of spin gapless semiconductors: the heusler compound Mn2CoAl, Phys. Rev. Lett. 110 (2012) 110401.
[31] Y. Du, G.Z. Xu, X.M. Zhang, Z.Y. Liu, S.Y. Yu, E.K. Liu, W.H. Wang, G.H. Wu, Crossover of magnetoresistance in the zero-gap half-metallic Heusler alloy Fe2CoSi, Epl 103 (2013) 37011.
[32] G.Y. Gao, K.L. Yao, Antiferromagnetic half-metals, gapless half-metals, and spin gapless semiconductors: the D03-type Heusler alloys, Appl. Phys. Lett. 103 (2013) 232409.
[33] S. Skaftouros, K. Ozdogan, E. Sasioglu, I. Galanakis, Search for spin gapless semiconductors: the case of inverse heusler compounds, Appl. Phys. Lett. 102 (2013) 022402.
[34] K. Ozdogan, E. Sasioglu, I. Galanakis, Slater-pauling behavior in LiMgPdSn-type multifunctional quaternary Heusler materials: half-metallicity, spin-gapless and magnetic semiconductors, J. Appl. Phys. 113 (2013) 193903.
[35] P. Hohenberg, W. Kohn, Inhomogeneous electron gas, Phys. Rev. B 136 (1964) B864-+.
[36] W. Kohn, L.J. Sham, Self-consistent equations including exchange and correlation effects, Phys. Rev. 140 (1965) 1133–1138.
[37] M.D. Segall, P.J.D. Lindan, M.J. Probert, C.J. Pickard, P.J. Hasnip, S.J. Clark, M.C. Payne, First-principles simulation: ideas, illustrations and the CASTEP code, J. Phys.: Condens. Matter 14 (2002) 2717–2744.
[38] J.P. Perdew, Y. Wang, Accurate and simple analytic representation of the electron-gas correlation-energy, Phys. Rev. B 45 (1992) 13244–13249.
[39] P.E. Blochl, O. Jepsen, O.K. Andersen, Improved tetrahedron method for brillouin-zone integrations, Phys. Rev. B 49 (1994) 16223–16233.
[40] C. Klewe, M. Meinert, J. Schmalhorst, G. Reiss, Negative spin polarization of Mn2VGa probed by tunnel magnetoresistance, J. Phys. Condens. Matter 25 (2013) 076001.
[41] X.T. Wang, Z.X. Cheng, J.L. Wang, G.D. Liu, A full spectrum of spintronic properties demonstrated by a C1b-type Heusler compound Mn2Sn subjected to strain engineering, J. Mater. Chem. C 4 (2016) 8535–8544.
[42] L. Zhang, X.T. Wang, Z.X. Cheng, Electronic, magnetic, mechanical, half-metallic and highly dispersive zero-gap half-metallic properties of rare-earth-element-based quaternary Heusler compounds, J. Alloys Compd. 718 (2017) 63–74.
[43] I. Galanakis, P.H. Dederichs, N. Papanikolaou, Slater-pauling behavior and origin of the half-metallicity of the full-Heusler alloys, Phys. Rev. B 66 (2002) 553–562.
[44] P. Alippi, P.M. Marcus, M. Scheffler, Strained tetragonal states and Bain paths in metals, Phys. Rev. Lett. 78 (1997) 3892–3895.
[45] B. Balke, G.H. Fecher, J. Winterlik, C. Felser, Mn3Ga, a compensated ferrimagnet with high Curie temperature and low magnetic moment for spin torque transfer applications, Appl. Phys. Lett. 90 (2007) 152504.
[46] K. Rode, N. Baadji, D. Betto, Y.C. Lau, H. Kurt, M. Venkatesan, P. Stamenov, S. Sanvito, J.M.D. Coey, Site-specific order and magnetism in tetragonal Mn3Ga thin films, Phys. Rev. B 87 (2013) 1853–1865.
[47] H. Kurt, K. Rode, M. Venkatesan, P. Stamenov, J.M.D. Coey, High spin polarization in epitaxial films of ferrimagnetic Mn3Ga, Phys. Rev. B 83 (2011) 287–292.
[48] L. Wollmann, G.H. Fecher, S. Chadov, C. Felser, A scheme for spin-selective electron localization in Mn3Ga Heusler material, J. Phys. D. Appl. Phys. 48 (2015) 16.
[49] W. Voigt, Lehrburch der Kristallphysik, Teubner, Leipzig, Lehrbuch der Kristallphysik, 1928.
[50] A. Reuss, Z. Angew, Math. Mech. Berechnung der Fliehgrenze von Mischkristallen auf Grund der Plastizittitsbedingung fiir Einkristalle. 9 (1929).
[51] E. Schreiber, O.L. Anderson, N. Soga, J.F. Bell, Elastic constants and their measurement, J Appl. Mech. 42 (1973) 747–748.
[52] S.I. Ranganathan, M. Ostoja-Starzewski, Universal elastic anisotropy index, Phys. Rev. Lett. 101 (2008) 055504.
[53] V.V. Bannikov, I.R. Shein, A.L. Ivanovskii, Electronic structure, chemical bonding and elastic properties of the first thorium-containing nitride perovskite TaThN3, Phys. Status Solidi-R 1 (2007) 89–91.